ARTICLE NO. 79-0343R

C80-025

Subsonic and Transonic Similarity Rules for Jet-Flapped Wings

20001
20016
20018

Henry W. Woolard*
U.S. Air Force Flight Dynamics Laboratory, Wright-Patterson Air Force Base, Ohio

Linear subsonic and nonlinear transonic similarity rules are presented for a finite-span jet-flapped wing with partial or full-span blowing. The nonlinear rules are new and the linear rules are more general than previous ones. The rules employ a new second-order jet momentum coefficient similarity parameter which includes the effect of the jet supply pressure ratio. The second-order effect is found to be significant only when convergent-jet-nozzle choking occurs at a low flight Mach number. Although the experimental data available for validation of the linear rules is sparse and uncertain, some comparisons are made and fair agreement is achieved. Camber line effects are found to be significant. There is no experimental data suitable for validation of the nonlinear rules. Motivation for this work is the possible use of pure jet flaps for maneuvering combat aircraft at high subsonic and transonic speeds.

Nomenclature

a = velocity of sound
A = wing aspect ratio
b = wing span
c = airfoil section chord
c_j = section isentropic momentum coefficient, $(\hat{\rho}_j \hat{U}_j h_j)\, \hat{U}_\infty / (\rho_\infty/2)\, U_\infty{}^2 c$
c_j^* = section nozzle exit momentum coefficient, $(\hat{\rho}_j \hat{U}_j h_j)\, \hat{U}_j / (\rho_\infty/2)\, U_\infty{}^2 c$
c_l = section lift coefficient, $c_{l_\Gamma} + c_{l_R}$
c_{l_Γ} = section circulation lift coefficient
c_{l_R} = section lift coefficient due to jet reaction
c_m = section pitching moment coefficient about the leading edge, nose-up positive
C_{D_i} = induced drag coefficient
C_L = wing lift coefficient, $C_{L_\Gamma} + C_{L_R}$
C_{L_Γ} = wing circulation lift coefficient
C_{L_R} = wing lift coefficient due to jet reaction
C_m = wing pitching moment coefficient about wing planform apex, nose-up positive, $C_{m_\Gamma} + C_{m_R}$
C_p = pressure coefficient, $(p-p_\infty)/(\rho_\infty/2)\, U_\infty{}^2$
$\mathfrak{D}$ = drag function
f_τ = wing thickness distribution function
f_κ = wing camber distribution function
h or h_{js} = jet sheet thickness at an arbitrary location
h_j = jet sheet thickness at nozzle (wing trailing edge)
H = section maximum camber height
I_G, I_F = See Eqs. (47) and (48)
k = $(\gamma+1) M_\infty{}^2 / U_\infty$
K_π = second-order correction factor, see Eqs. (A18) and (A19)
$\mathfrak{L}$ = lift function
M = Mach number
$\mathfrak{M}$ = pitching moment function
n,s = natural coordinates
p = static pressure
P = total pressure
$\mathcal{P}$ = pressure function
r = local radius of curvature in jet sheet (see Fig. A1)
R = radius of curvature at center of jet sheet (see Fig. A1)
s = stretching factor (with appropriate subscript) as defined in Eq. (10)
S = wing area
S^* = normalized wing area, $2S/bc_r$
t = maximum thickness of a wing section
u = local velocity parallel to x or s
$\hat{U}_j$ = uniform jet velocity at nozzle (wing trailing edge)
$\hat{U}_\infty$ = jet isentropic expansion velocity corresponding to isentropic expansion of jet to freestream static pressure
U_∞ = freestream velocity
x,y,z = Cartesian coordinate system with positive x extending in the direction of the freestream (see Fig. 1).
$\tilde{x},\tilde{y},\tilde{z}$ = Cartesian coordinate system in the transformed space according to Eq. (10)
x^*,y^*,z^* = normalized coordinates, $x/c_r, 2y/b, z/c_r$
$\lvert y_I \rvert, \lvert y_O \rvert$ = inboard and outboard limits of spanwise blowing (see Fig. 1)
α = angle of attack relative to the camber line chord
$\breve{\alpha}$ = angle of attack relative to the chord line used in specifying the airfoil coordinates
$\breve{\alpha}'$ = angle of attack relative to an arbitrary reference line
$\beta_\infty{}^2$ = $1 - M_\infty{}^2$
γ = ratio of specific heats
δ_j = jet flap deflection angle at wing trailing edge, measured positive downward relative to wing chord (see Fig. 1)
ϵ = an arbitrary constant for linear flow; $= U_\infty k$ for nonlinear flow
θ = local streamline slope in a plane y equals a constant, assuming negligible lateral flow (see Fig. 1)
θ_i = upwash angle for induced drag calculations
κ = section camber ratio, H/c
λ_c = ratio of tip-to-root chord
λ_t = ratio of tip-to-root thickness
λ_κ = ratio of tip-to-root maximum camber
Λ = wing sweepback angle
ρ = density
σ = arbitrary parameter, may be τ, κ, α, θ_j, or δ_j
τ = wing section thickness ratio, t/c

Presented as Paper 79-0343 at the 17th Aerospace Sciences Meeting, New Orleans, La., Jan. 15-17, 1979; submitted March 20, 1979; revision received July 2, 1979. Reprints of this article may be ordered from AIAA Special Publications, 1290 Avenue of the Americas, New York, N.Y. 10019. Order by Article No. at top of page. Member price $2.00 each, nonmember, $3.00 each. **Remittance must accompany order.**

Index categories: Aerodynamics; Subsonic Flows; Transonic Flows.

*Aerospace Engineer, Flight Control Division, Control Dynamics Branch (FGC). Associate Fellow AIAA.

ϕ = perturbation velocity potential, $\Phi = U_\infty x + \phi$
Φ = total velocity potential
Ω = $\phi / U_\infty z$
ω = arbitrary constant (see text)

Subscripts, Superscripts, etc.

j = quantity associated with the jet sheet at the wing trailing edge
js = quantity associated with the jet sheet at an arbitrary location on the sheet
R = quantity due to the jet reaction
o = quantity on the centerline of the jet sheet
u,l = upper and lower stream surface for either the wing or jet sheet, respectively
r = wing root chord
x,y,z = partial derivative except when subscripting s
w = wing quantity
Γ = quantity due to the wing circulation lift
∞ = freestream conditions
$( )^*$ = sonic conditions
$'$ = perturbation quantity (except for α')
$\tilde{}$ = quantity in the transformed space according to Eqs. (10)
$\hat{}$ = a quantity within the jet sheet interior (see Fig. A1)
$< >$ = a mean value

Introduction

WITH reference to Fig. 1, consider the flow about a finite-span pure† jet-flapped wing with partial or full-span blowing‡ of the jet sheets. The motivation for study of this flow is the possible use of jet flaps for maneuvering combat aircraft at high subsonic and transonic speeds. This contrasts with the more conventional application of the jet-flap supercirculation principle wherein the jet sheets are employed to augment the lift of a mechanical flap during the takeoff or landing flight phase of an aircraft. In this latter application, compressibility effects are of secondary importance.

Assuming small flow perturbations and restriction to wings without dihedral and twist, linear subsonic and nonlinear transonic similarity rules are derived herein for the subject flow. In developing these similarity rules a new jet sheet compatibility condition, which is of second order relative to the jet sheet internal flow, is derived. The new compatibility condition yields a jet momentum coefficient similarity parameter differing from the conventional parameter in that it includes the effect of the jet supply pressure ratio. In applying the similarity laws, particular attention is given to camber line effects which heretofore have been unimportant in applications involving jet-augmented mechanical flaps.

The nonlinear transonic similarity rules derived herein for jet-flapped wings are new (to the best of the author's knowledge). For the linear subsonic case, however, similarity laws for jet-flapped wings previously have been presented by Siestrunk,[1] Levinsky,[2] Elzweig,[3] and probably others. Each of the aforementioned investigators employs a different scaling law, and only Levinsky considers the finite-span wing; the other treatments are for two-dimensional flow. The present treatment is more general than the foregoing ones in that it applies to both two- and three-dimensional wings, allows for the selection of the scaling law most appropriate for the particular problem under consideration, and includes a second-order scaling of the jet internal flow that accounts for the jet supply pressure ratio. The laws employed herein reduce to those of the aforementioned investigators upon appropriate selection of the parameters.

†That is, a wing employing jet sheets alone, unassisted by mechanical devices such as flaps or ailerons.

‡For convenience in discussion, reference to a "blown" or "unblown" wing will connote, respectively, a wing with or without jet flaps operating.

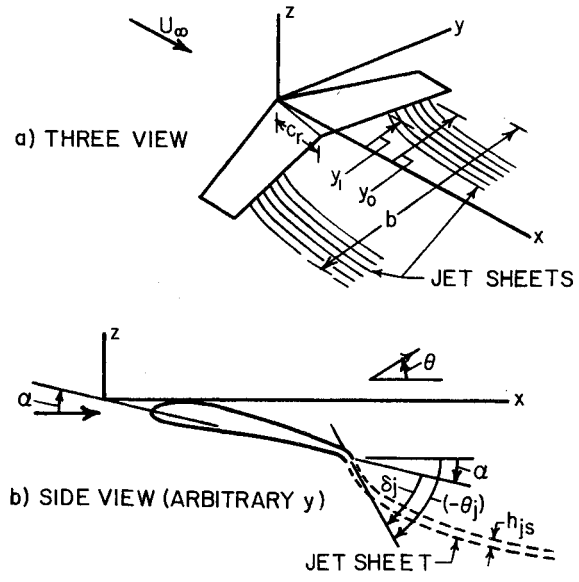

Fig. 1 Illustration of flow problem and notation.

As a consequence of the assumption of small perturbations, application of the present results obviously is limited to small thickness and camber ratios, small angles of attack, and small jet deflection angles.

This paper is based on an Air Force Technical Report[4] published by the author. Greater detail may be found in that document.

Analysis

The present analysis is limited to a specific class of wings having neither twist nor dihedral and for which the half-span planform is a trapezoid with the root and tip chords parallel, the wing section geometries affine to each other at varying spanwise stations, and the section characteristic dimensions (chord, thickness, camber height, etc.) varying linearly in the spanwise direction. For convenience this class of wings will be referred to herein as "trapezoidal," although the terminology generally refers only to wing planform geometry. Similarity rules may be developed for a broader class of wing geometries with a correspondingly increased complexity. However, since many actual aircraft wings are trapezoidal or nearly trapezoidal in the aforementioned sense, it is convenient for the sake of brevity and definiteness to restrict the presentation to this class of wings. The geometry for these wings may be given by

$$z_w^* = \sigma F(x^*, y^*; A\tan\Lambda, \lambda_c, \lambda_t, \lambda_\kappa, \tau_r/\sigma, \kappa_r/\sigma, \alpha/\sigma) \tag{1}$$

where

$$F \equiv \pm (\tau_r/\sigma) f_\tau (x^*, y^*; A\tan\Lambda, \lambda_c, \lambda_t) + (\kappa_r/\sigma) f_\kappa (x^*, y^*; A\tan\Lambda, \lambda_c, \lambda_\kappa) - (\alpha/\sigma) x^* \tag{2}$$

with the spanwise blowing distribution given by

$$c_j = c_j(y_j^*); \delta_j = \delta_j(y_j^*) \tag{3}$$

The parameter σ may be selected to be any one of the parameters τ_r, κ_r, α, θ_j, or δ_j depending upon the type of problem under consideration.

Deflected ailerons and flaps may be treated by introducing functions analogous to f_τ and f_κ which are dependent upon the associated geometries. The concern here, however, is for pure jet-flapped wings.

The governing partial differential equation for the perturbation velocity potential[5] is

$$\beta_\infty^2(\partial^2\phi/\partial x^2)+\partial^2\phi/\partial y^2+\partial^2\phi/\partial z^2=jk(\partial\phi/\partial x)(\partial^2\phi/\partial x^2) \tag{4}$$

where for linear subsonic compressible flow $j=0$, and for nonlinear transonic flow $j=1$.

The shock wave compatibility condition[5] is

$$\beta_\infty^2(\Delta\phi_x)^2+(\Delta\phi_y)^2+(\Delta\phi_z)^2=k(\tfrac{1}{2})(\phi_{x_1}+\phi_{x_2})(\Delta\phi_x)^2 \tag{5}$$

where the subscripts x, y, and z denote partial derivatives, and Δ denotes a jump in the modified quantity such that if "1" and "2" denote, respectively, upstream and downstream conditions relative to the shock $\Delta\phi_x=\phi_{x_1}-\phi_{x_2}$, etc.

If the lateral flow velocity perturbations are assumed to be negligible compared to the vertical and longitudinal ones, the jet sheet compatibility condition as derived in the Appendix is

$$U_\infty^{-1}(\partial\phi/\partial x)_{z=0}=(c/4)(\partial\theta_{js}/\partial x)K_\pi c_j \tag{6}$$

where K_π is the jet sheet second-order correction factor defined by Eqs. (A18) and (A19) in the Appendix.

The boundary conditions at $x=-\infty$ are

$$\phi_x=\phi_y=\phi_z=0 \tag{7}$$

The wing surface boundary condition is

$$(\partial\phi/\partial z)_{z=0}=U_\infty\sigma(\partial/\partial x^*)F(x^*,y^*;\tau_r/\sigma,\kappa_r/\sigma,\alpha/\sigma) \tag{8}$$

The jet sheet boundary condition is

$$\theta_{js}(x^*,y^*,0)=(\partial\phi/\partial z)_{z=0}/U_\infty \tag{9}$$

We now introduce the transformations

$$\begin{aligned}\tilde{x}\quad&=s_x x,\tilde{y}=s_y y,\tilde{z}=s_z z,\tilde{\phi}=s_\phi\phi\\ \tilde{U}_\infty\quad&=s_u U_\infty,\tilde{\beta}_\infty=s_\beta\beta_\infty,(\tilde{U}_\beta\tilde{k})=s_k(U_\infty k)\end{aligned} \tag{10}$$

Flow similarity is achieved by determining appropriate values of the s-stretching factors as dictated by the governing equations and boundary conditions.

The boundary conditions specified by Eq. (7) are obviously preserved by the transformations of Eq. (10).

We consider first the constraints imposed upon the stretching factors by the governing partial differential equation (4) and the shock compatibility condition [Eq. (5)]. If the transformations of Eq. (10) are applied to the aforementioned equations, it is found the following conditions must be satisfied in order for the governing equations to be of the same form in the two spaces,

$$(s_x^2/s_\beta^2)=s_y^2=s_z^2=s_x^2(s_u s_x/s_\phi)/(\tilde{\epsilon}/\epsilon) \tag{11}$$

where

$$\tilde{\epsilon}/\epsilon=\text{an arbitrary constant (linear)} \tag{12}$$

$$\tilde{\epsilon}/\epsilon=(\tilde{U}_\infty\tilde{k}/U_\infty k)\qquad\text{(nonlinear)} \tag{13}$$

The freedom of choice in selecting the parameter $(\tilde{\epsilon}/\epsilon)$ in the linear case introduces the option of an additional degree of freedom in the scaling. This option is a well-known property of subsonic scaling laws (see, e.g., Ref. 5 or any standard textbook).

From the first and third terms in Eq. (11) it is easily shown that

$$(s_u s_x/s_\phi)=s_\beta(s_u s_z/s_\phi) \tag{14}$$

In the analysis (s_u/s_ϕ) always appears in one of the parenthetical combinations shown in Eq. (14). The stretching factors s_u and s_ϕ therefore need not be determined separately and the quantities $(s_u s_x/s_\phi)$ and $(s_u s_z/s_\phi)$ may be treated as unknown parameters.

Substituting Eq. (14) in Eq. (11), and noting that $(s_\phi/s_u s_z)=\tilde{\Omega}/\Omega$, yields

$$s_x^2/s_\beta^2=s_y^2=s_z^2=s_x^2 s_\beta/(\tilde{\epsilon}/\epsilon)(\tilde{\Omega}/\Omega) \tag{15}$$

Equations (15) define three equations relating the stretching factors. This set of equations may have a variety of forms, depending upon the algebraic manipulations performed. The forms used herein are

$$s_y(\tilde{\epsilon}\tilde{\Omega}/\epsilon\Omega)^{1/3}=s_x \tag{16}$$

$$s_z(\tilde{\epsilon}\tilde{\Omega}/\epsilon\Omega)^{1/3}=s_x \tag{17}$$

$$\tilde{\Omega}/\Omega=(\tilde{\beta}_\infty/\beta_\infty)^3(\epsilon/\tilde{\epsilon}) \tag{18}$$

The principal linear dimensions of the original and transformed wings are related by

$$\begin{aligned}&\tilde{c}_r=s_x c_r;\tilde{b}=s_y b;\tilde{t}_r=s_z t_r\\ &\tilde{y}_I=s_y y_I;\tilde{y}_O=s_y y_O\end{aligned} \tag{19}$$

yielding

$$\begin{aligned}&\tilde{x}^*=x^*;\tilde{y}^*=y^*;(\tilde{\epsilon}\tilde{\Omega})^{1/3}\tilde{z}^*=(\epsilon\Omega)^{1/3}z^*\\ &\tilde{y}_I^*=y_I^*;\tilde{y}_O^*=y_O^*\end{aligned} \tag{20}$$

The transformation relations of Eq. (10) and the similarity conditions of Eqs. (11) yield the following relations for the sweepback angles and the aspect ratios

$$(\tan\tilde{\Lambda})/\tilde{\beta}_\infty=(\tan\Lambda)/\beta_\infty \tag{21}$$

$$\tilde{\beta}_\infty\tilde{A}=\beta_\infty A \tag{22}$$

Any one of the parameters s_x, s_y, or s_z in Eq. (19) may be assigned an arbitrary value. For unit values of s_x, s_y, and s_z, respectively, Eqs. (19) indicate that wings of identical root chord, span, or root thickness respectively are being compared in the original and transformed spaces. A common selection is $s_x=1.0$.

To achieve manageable results, it is necessary to assume that $\tilde{f}_\tau=f_\tau$, $\tilde{f}_\kappa=f_\kappa$, and $\tilde{F}=F$. That is, the analysis is confined to families of wings defined by these constraints. The wing geometry in the transformed space then becomes

$$\tilde{z}_w^*=\tilde{\sigma}F(\tilde{x}^*,\tilde{y}^*;\tilde{A}\tan\tilde{\Lambda},\tilde{\lambda}_c,\tilde{\lambda}_t,\tilde{\lambda}_k,\tilde{\tau}_r/\tilde{\sigma},\tilde{\kappa}/\tilde{\sigma},\tilde{\alpha}/\tilde{\phi}) \tag{23}$$

where

$$\begin{aligned}F\equiv{}&\pm(\tilde{\tau}_r/\tilde{\sigma})f_\tau(\tilde{x}^*,\tilde{y}^*;\tilde{A}\tan\tilde{\Lambda},\tilde{\lambda}_c,\tilde{\lambda}_t)\\ &+(\tilde{\kappa}_r/\tilde{\sigma})f_\kappa(\tilde{x}^*,\tilde{y}^*;\tilde{A}\tan\tilde{\Lambda},\tilde{\lambda}_c,\tilde{\lambda}_k)-(\tilde{\alpha}/\tilde{\sigma})\tilde{x}^*\end{aligned} \tag{24}$$

with

$$\tilde{c}_j=\tilde{c}_j(\tilde{y}_j^*);\tilde{\delta}_j=\tilde{\delta}_j(\tilde{y}_j^*) \tag{25}$$

The equality of the f's requires [compare Eqs. (2) and (24)] that

$$\tilde{A}\tan\tilde{\Lambda}=A\tan\Lambda \tag{26}$$

$$\tilde{\lambda}_c=\lambda_c,\tilde{\lambda}_t=\lambda_t,\tilde{\lambda}_\kappa=\lambda_\kappa \tag{27}$$

The equality of the F's, in combination with the equality of the f's, requires that

$$\tilde{\tau}_r/\tilde{\sigma}=\tau_r/\sigma \tag{28}$$

$$\tilde{\kappa}_r/\tilde{\sigma}=\kappa_r/\sigma \tag{29}$$

$$\tilde{\alpha}/\tilde{\sigma}=\alpha/\sigma \tag{30}$$

It is apparent that the transformations of Eq. (10) are consistent with the conditions of Eqs. (26) and (27) which are a consequence of restricting the analysis to a family of wings. Also note that Eq. (26) is equivalent to the pair of Eqs. (21) and (22).

The boundary condition on the wing in the transformed space is given by

$$(\partial\tilde{\phi}/\partial\tilde{z})_{\tilde{z}=0}=\tilde{U}_\infty\tilde{\sigma}(\partial/\partial\tilde{x}^*)\tilde{F}(\tilde{x}^*,\tilde{y}^*;\text{---}) \tag{31}$$

Applying the transformations of Eq. (10) to the wing boundary condition in the original space yields

$$(s_z/s_\phi)(\partial\tilde{\phi}/\partial\tilde{z})_{\tilde{z}=0}=(\tilde{U}_\infty/s_u)\sigma(\partial/\partial\tilde{x}^*)F(\tilde{x}^*,\tilde{y}^*;\text{---}) \tag{32}$$

Recalling that $F=\tilde{F}$, Eqs. (31) and (32) require that $\tilde{\sigma}/\sigma) = (s_\phi/s_u s_z)$. This condition, an invariant of the transformation, may be written as $(\tilde{\Omega}/\tilde{\sigma}) = (\Omega/\sigma)$. In applying the similarity laws, the aforementioned invariant is frequently employed in the form

$$(\tilde{\Omega}/\tilde{\sigma})^\omega=(\Omega/\sigma)^\omega \tag{33}$$

where the value of ω is arbitrarily selected to achieve a particular desired form for the invariant parameters in the final formation of the similarity rules. Common choices are (-1) and $(2/3)$ for subsonic and transonic flows, respectively.

Assuming negligible lateral curvature, the streamline slopes in the two spaces are

$$\theta=(\partial\phi/\partial z)/U_\infty \tag{34}$$

$$\tilde{\theta}=(\partial\tilde{\phi}/\partial\tilde{z})/\tilde{U}_\infty=(\tilde{\Omega}/\Omega)(\partial\phi/\partial z)/U_\infty \tag{35}$$

yielding the result $(\tilde{\Omega}/\tilde{\theta}) = (\Omega/\theta)$, where, as for Eq. (33), we employ the form

$$(\tilde{\Omega}/\tilde{\theta})^\omega=(\Omega/\theta)^\omega \tag{36}$$

Since the jet sheet is a stream surface, Eq. (36) applies to the jet sheet slopes θ_{js} and $\tilde{\theta}_{js}$. A basic parameter for the jet sheet, however, is the slope θ_j at the wing trailing edge. Applying Eq. (36) to θ_j and $\tilde{\theta}_j$ yields

$$(\tilde{\Omega}/\tilde{\theta}_j)^\omega=(\Omega/\theta_j)^\omega \tag{37}$$

where

$$\theta_j=-(\alpha+\delta_j),\tilde{\theta}_j=-(\tilde{\alpha}+\tilde{\delta}_j) \tag{38}$$

When σ is selected to be δ_j, it is easily shown through the use of Eqs. (30) and (38) that an optional form for Eq. (37) is

$$(\tilde{\Omega}/\tilde{\delta}_j)^\omega=(\Omega/\delta_j)^\omega \quad (\text{For } \sigma=\delta_j) \tag{39}$$

The compatibility condition for the jet sheet in the original space is given by Eq. (6); in the transformed space it is

$$U_\infty^{-1}(\partial\tilde{\phi}/\partial\tilde{x})_{\tilde{z}=0}=(\tilde{c}/4)(\partial\tilde{\theta}_{js}/\partial\tilde{x})\tilde{K}_\pi\tilde{c}_j \tag{40}$$

Applying the transformations of Eqs. (10) to Eq. (6) and employing Eq. (17) to substitute for the ratio (s_z/s_x) yields

$$U_\infty^{-1}(\partial\tilde{\phi}/\partial\tilde{x})_{\tilde{z}=0}=(\tilde{c}/4)(\Omega\epsilon/\tilde{\Omega}\tilde{\epsilon})^{1/3}(\partial\tilde{\theta}_{js}/\partial\tilde{x})K_\pi c_j \tag{41}$$

From Eqs. (40) and (41)

$$(\tilde{\epsilon}\tilde{\Omega})^{1/3}\tilde{K}_\pi\tilde{c}_j=(\epsilon\Omega)^{1/3}K_\pi c_j \tag{42}$$

where, from Eqs. (18, 33, 37, and 39) the parameter $(\tilde{\Omega}/\Omega)$ required for Eq. (42) is given by any one of the following equations

$$\begin{aligned}&\tilde{\Omega}/\Omega=\tilde{\beta}_\infty^3\epsilon/\beta_\infty^3\tilde{\epsilon}\\&\tilde{\Omega}/\Omega=\tilde{\sigma}/\sigma;\tilde{\Omega}/\Omega=\tilde{\theta}_j/\theta_j\end{aligned} \tag{43}$$

Equations (42) and (43) are the invariant conditions for the jet momentum coefficient. Note that if σ is selected to be other than δ_j or θ_j (with $\tilde{\sigma}$ selected correspondingly) Eq. (43) permits three optional choices for $\tilde{\Omega}/\Omega$, but if σ is selected to be δ_j or θ_j (with $\tilde{\sigma}$ selected correspondingly) only two options are available for $(\tilde{\Omega}/\Omega)$.

The relation between the pressure coefficients at corresponding points in the two spaces is given by

$$\tilde{C}_p=(s_\phi/s_u s_x)C_p \tag{44}$$

The factor $(s_\phi/s_u s_x)$ in Eq. (44) can be written as $(s_\phi/s_u s_x)^{2/3}$ $(s_\phi/s_u s_x)^{1/3}$ and appropriately manipulated to give

$$(s_\phi/s_u s_x)=(\tilde{\Omega}/\Omega)^{2/3}(\epsilon/\tilde{\epsilon})^{1/3} \tag{45}$$

Substituting Eq. (45) in Eq. (44) and indicating the functional dependence of the pressure coefficient yields

$$\begin{aligned}&(\epsilon/\Omega^2)^{1/3}C_p[x^*,y^*,(\epsilon\Omega)^{1/3}z^*;I_G,I_F]\\&=(\tilde{\epsilon}/\tilde{\Omega}^2)^{1/3}\tilde{C}_p[\tilde{x}^*,\tilde{y}^*,(\tilde{\epsilon}/\tilde{\Omega})^{1/3}\tilde{z}^*;\tilde{I}_G,\tilde{I}_F]\end{aligned} \tag{46}$$

where

$$I_G\equiv\dot{y}^*{}_I,y^*{}_O,\lambda_c,\lambda_t,\lambda_\kappa \tag{47}$$

$$I_F\equiv(\tan\Lambda)/\beta_\infty,\beta_\infty A,\tau_r/\sigma,\kappa_r/\sigma,\alpha/\sigma,(\Omega/\sigma)^\omega,(\Omega/\theta_j)^\omega,(\epsilon\Omega)^{1/3}(K_\pi c_j) \tag{48}$$

and K_π is given by Eqs. (A18) and (A19) in the Appendix. The parameter σ may be selected as any one of the parameters τ_r, κ_r, α, θ_j, or δ_j depending upon the type of problem under consideration. The form of the parameter ϵ (and hence $\tilde{\epsilon}$) is arbitrary for subsonic linear flow, and, in accordance with Eq. (13), is $\epsilon=U_\infty k(\tilde{\epsilon}=\tilde{U}_\infty k)$ for nonlinear transonic flow. The optional choices for the form of Ω (and hence $\tilde{\Omega}$) are specified by Eq. (43). The value of ω is arbitrary and depends upon the type of problem under consideration. Common selections for ω are (-1) and $(\frac{2}{3})$ for subsonic and transonic flow, respectively. A selection for σ that yields unity for any one of the ratioed parameters in Eq. (48) indicates a lack of an invariance constraint on that ratio. There is no unique combination of the similarity parameters appearing in Eqs. (46) and (48). The parameters shown may be rearranged to give a wide variety of combinations by appropriate manipulation of Eqs. (28, 30, 26, and 43) [noting the equivalence of the ratios on the right-hand side of Eq. (43)]. Such a procedure is permissible providing the total number of

invariant parameters remains unchanged in any rearrangement.

The following aerodynamic coefficients are defined

$$C_L = C_{L_\Gamma} + C_{L_R} \tag{49}$$

$$C_{L_\Gamma} = (bc_r/2S) \int \int_{S^*} (C_{p_l} - C_{p_u})\, dx^* dy^* \tag{50}$$

$$C_{L_R} = -(bc_r/2S) \int_{-1}^{1} c_j \theta_j (c/c_r)\, dy^* \tag{51}$$

$$C_{D_i} = -\theta_i C_L \tag{52}$$

$$C_m = C_{m_\Gamma} + C_{m_R} \tag{53}$$

$$C_{m_\Gamma} = -(bc_r/2S) \int_S \int_* x^* (C_{p_l} - C_{p_u})\, dx^* dy^* \tag{54}$$

$$C_{M_R} = (bc_r/2S) \int_{-1}^{1} x_j^* c_j \theta_j (c/c_r)\, dy^* \tag{55}$$

where $(-\theta_i)$ is an appropriate downwash angle and the small-angle assumption $(\sin\theta_j = \theta_j)$ has been employed in the jet reaction coefficients.

Application of the similarity rules yields the following results

$$C_p(x^*, y^*, 0) = (\Omega^2/\epsilon)^{1/3} \mathcal{P}(x^*, y^*, 0; I_G I_F) \tag{56}$$

$$C_L = (\Omega^2/\epsilon)^{1/3} \mathcal{L}(I_G, I_F) \tag{57}$$

$$C_{L_\Gamma} = (\Omega^2/\epsilon)^{1/3} \mathcal{L}_\Gamma(I_G, I_F) \tag{58}$$

$$C_{L_R} = (\Omega^2/\epsilon)^{1/3} \mathcal{L}_R(I_G, I_F) \tag{59}$$

$$C_{D_i} = (\Omega^5/\epsilon)^{1/3} \mathcal{D}_i(I_G, I_F) \tag{60}$$

$$C_m = (\Omega^2/\epsilon)^{1/3} \mathcal{M}(I_G, I_F) \tag{61}$$

$$C_{m_\Gamma} = (\Omega^2/\epsilon)^{1/3} \mathcal{M}_\Gamma(I_G, I_F) \tag{62}$$

$$C_{m_R} = (\Omega^2/\epsilon)^{1/3} \mathcal{M}_R(I_G, I_F) \tag{63}$$

where I_G and I_F are given by Eqs. (47) and (48), respectively, and $\mathcal{L} = \mathcal{L}_\Gamma + \mathcal{L}_R$ and $\mathcal{M} = \mathcal{M}_\Gamma + \mathcal{M}_R$.

Since in the linear case the form of ϵ may be selected arbitrarily, it is of interest to examine the consequences of several choices for this parameter. For $\epsilon = \Omega^2$ $(\bar{\epsilon} = \bar{\Omega}^2)$, Eq. (46) shows that the pressure coefficients at affinely related points in the original and transformed spaces are identical. For $\epsilon = \beta_\infty{}^3$, Eq. (18) shows that $\Omega = \bar{\Omega}$, from which it follows from Eq. (33) that $\sigma = \bar{\sigma}$, and from Eq. (37) that $\theta_j = \bar{\theta}_j$. Finally, Eqs. (28-30) show that the thickness ratios, camber ratios, and angles of attack are identical in the original and transformed spaces. For $\epsilon = U_\infty k$, Eqs. (12) and (13) show that the similarity parameters are identical for both linear and nonlinear flows.

For both blown and unblown wings, the relations in this paper may be shown to reduce those of various other investigators by taking $K_\pi = 1$ and by appropriate selection of Ω, ϵ, and σ, and, perhaps, some additional manipulation of the invariants. See Woolard[4] for details.

Comparison with Experiment

As noted previously, for jet-flapped wings there is no experimental data of appropriate configurational simplicity and of sufficient generality in parametric variations to permit validation of the nonlinear rules (to the knowledge of this writer). The data available for validation of the linear rules are rather sparse, lacking in sufficient detail, and plagued with uncertainties regarding wind tunnel wall corrections. Nevertheless some limited comparisons are made in this section. The data sources selected for comparisons are: 1) Air Force/Northrop tests,[6] 2) Air Force/Convair/Canadian tests,[7] and 3) French/O.N.E.R.A. tests.[8] The first two test series are for two-dimensional airfoils, whereas the third is for a finite-aspect-ratio wing employing a semispan test arrangement. Additional details on the aforementioned tests may be found in references cited by Woolard.[4]

It is important to note that all the theoretical results presented herein are completely theoretical. This contrasts to the practice of some investigators who, in the process of comparing their linear similarity results with experiment, arbitrarily adjust the zero Mach number case to obtain more favorable agreement in the high Mach number region.

The Air Force/Northrop tests[6] were conducted at the Arnold Engineering Development Center (AEDC) in the 4T wind tunnel. The model tested was a modified NACA 64A406 airfoil section with a 10 in. chord, a 20 in. span, and was mounted between two large end plates. Forces and moments were not measured directly, but were deduced from measured surface pressures. The data presented[6] was not corrected for tunnel or end plate interference effects. For the present comparisons, therefore, an approximate correction was derived by Woolard.[4]

Taking $\epsilon = \beta_\infty{}^3$, $\sigma = \alpha$, $\omega = -1$, and selecting $\Omega = \beta^3/\epsilon$ from the options of Eqs. (43), Eq. (57) yields for the two-dimensional lift coefficient subsonic similarity relation

$$c_l = \beta_\infty^{-1} [\kappa c_{l_\kappa}(\beta_\infty K_\pi c_j) + \alpha c_{l_\alpha}(\beta_\infty K_\pi c_j) + \delta_j c_{l_{\delta_j}}(\beta_\infty K_\pi c_j)] \tag{64}$$

The κ, α, and δ_j subscripts on c_l denote partial derivatives with respect to the subscript. Methods for determining the κ derivative for incompressible flow are given by Woolard,[9] while methods for the α and δ_j derivatives are given by Spence.[10]

The consequences of Eq. (64) are compared with the Air Force/Northrop experiments[6] in Fig. 2 for a 35 deg jet-flap deflection. The experimental data shown are for a constant geometrical angle of attack, $\alpha_g = -0.63$ deg, which differs from the actual aerodynamic angle of attack due to tunnel interference effects. Corrected aerodynamic angles of attack due to tunnel interference were obtained by a method derived by Woolard.[4] The resulting angle of attack values at Mach numbers of 0.7 and 0.8 are -1.44 and -1.55 deg, respectively, for $c_j = 0$, and -2.04 and -2.16 deg, respectively, for $c_j = 0.0225$. The theoretical results directly comparable to experiment are shown by the solid symbols. Similarly oriented flags on the symbols denote identical angles of attack. The theoretical lift coefficient variation with Mach number at a constant angle of attack is shown by the solid lines in Fig. 2. The constant angle of attack is the average of the experimental aerodynamic angles of attack for $M_\infty = 0.7$ and 0.8. Although the quantitative agreement between theory and experiment for the blowing case is not completely satisfactory, the theory does indicate the general trend.

The relative importance of the jet sheet second-order effect can be seen in Fig. 2 by comparing the first-order dashed line curve for $K_\pi = 1.0$ with the second-order solid line curve for variable K_π. It is seen that the second-order effect is significant in this case. The second-order effect becomes significant because choking (where K_π deviates from unity) occurs at a relatively low freestream Mach number.

The dashed dot curve in the lower portion of Fig. 2 shows the incremental lift coefficient due to camber with blowing $(\Delta c_l)_\kappa$, where

$$(\Delta c_l)_\kappa \equiv (\kappa/\beta_\infty)[c_{l_\kappa}(\beta_\infty K_\pi c_j) - c_{l_\kappa}(0)] \tag{65}$$

Because of its relatively small magnitude in applications involving jet-augmented mechanical flaps the incremental

blown camber line contribution is usually neglected in those cases. For the example of Fig. 2, however, although $(\Delta c_l)_\kappa$ is small, it is of sufficient relative magnitude to warrant its inclusion.

The Air Force/Convair/Canadian tests[7] were conducted in the Canadian National Aeronautical Establishment (NAE) two-dimensional, high Reynolds number, transonic wind tunnel at Ottawa, Ontario. Several different jet-flapped supercritical-type airfoils were tested in the series of tests reported in the references cited by Woolard.[4] The airfoil with which comparisons are made herein was designated as an NAE 001002 airfoil, possessed considerable aft camber, had a chord of 15 in., and a jet deflection angle of 30 deg. Some test results for this model are briefly reported upon by Peake and associates.[7] The test data with which comparisons are made herein, however, were taken from an NAE internal test report of limited distribution. In the NAE tests, forces and moments were measured by side-wall balances with supplementary data

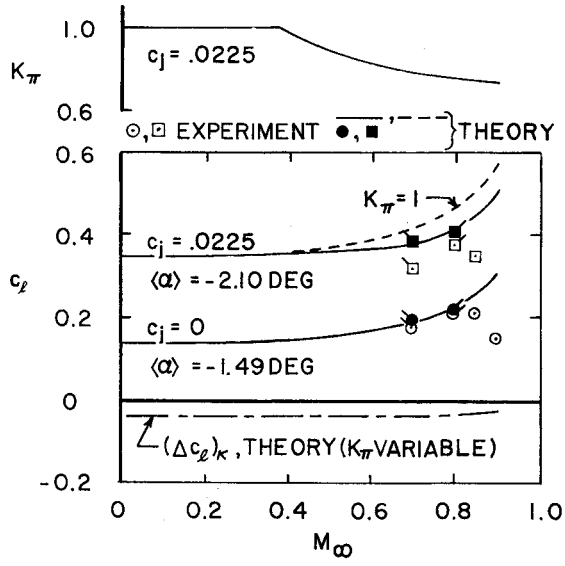

Fig. 2 Comparison of theory and experiment for Air Force/Northrop tests on modified NACA 64A406 airfoil section,[6] $\alpha_g = -0.63$ deg, $\delta_j = 35$ deg, $h_j/c = 0.0020$.

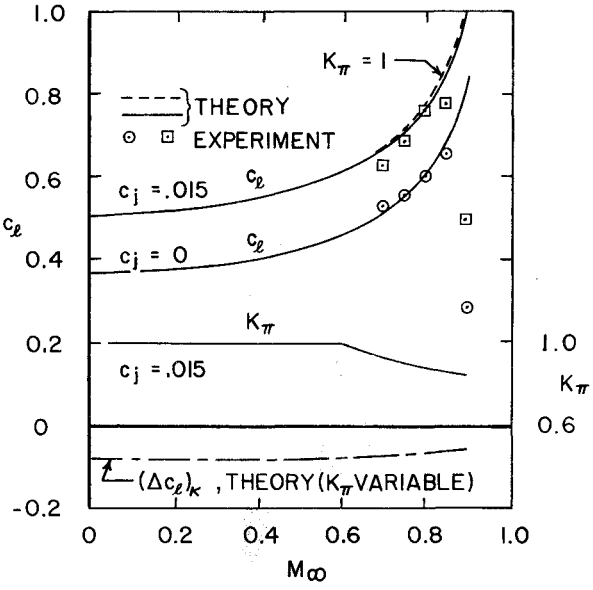

Fig. 3 Comparison of theory and experiment for Air Force/Convair/Canadian tests on NAE 001002 airfoil section,[7] $\alpha' = -0.66$ deg, $\delta_j = 30$ deg, $h_j/c = 0.0030$.

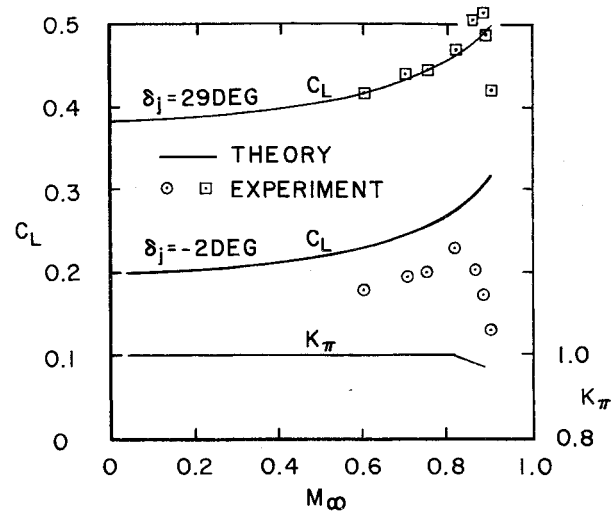

Fig. 4 Comparison of theory and experiment for French O.N.E.R.A. tests on finite-span wing,[8] $\alpha = 3$ deg, $c_j = 0.023$, $A = 3.4$, $h_j/c = 0.0080$.

taken by a wake survey rake. A tunnel-interference angle of attack correction of the same form as that used by Woolard,[4] but differently derived, was applied.

A comparison of the results given by the subsonic similarity relation of Eq. (64) with some NAE test data is given in Fig. 3. Figure 3 shows that rather good agreement is obtained for subcritical Mach numbers. Note also that the lift coefficient increment due to the blown camber line is significant.

As before, the relative importance of the jet sheet second-order effect can be seen by comparing the dashed line curve for $K_\pi = 1.0$ with the solid line curve for the variable K_π shown. In this case the second-order effect is negligible due to the fact that nozzle choking occurred at a relatively high freestream Mach number.

The French O.N.E.R.A. tests[8] were conducted on a half-span rectangular model of aspect ratio 3.4. The airfoil section is a NACA 64A010 airfoil truncated and modified at the 88% chord position yielding an 11.4% thick airfoil. Further details on the model and facility were not available.

In applying the subsonic similarity law, Hartunian's theory[11] for a finite-span jet-flapped wing is employed to obtain the wing characteristics at zero Mach number. Taking $\epsilon = \beta_\infty^3$, $\Omega = 1$, $\sigma = \alpha$, $\omega = -1$, Hartunian's lift coefficient relation,[11] Eqs. (57, 37, and 52) yield respectively the following similarity relations

$$C_L = \beta_\infty^{-1}\left[\frac{\alpha c_{l_\alpha}(\beta_\infty K_\pi c_j) + \delta_j c_{l_{\delta_j}}(\beta_\infty K_\pi c_j)}{1 + \dfrac{c_{l_{\delta_j}}(\beta_\infty K_\pi c_j)}{\pi\beta_\infty A + 2\beta_\infty K_\pi c_j}}\right] \tag{66}$$

$$(-\theta_i) = (-\theta_i)_{M_\infty = 0}; \quad C_{D_i} = (-\theta_i)_{M_\infty = 0} C_L \tag{67}$$

where the subscripts on c_l denote partial derivatives with respect to the subscript.

A comparison of the lift coefficient scaling given by Eq. (66) with the O.N.E.R.A. experiments[8] appears in Fig. 4, where reasonably good agreement is obtained for a jet deflection angle of 29 deg, but poorer agreement is obtained for $\delta_j = -2$ deg. Apparently the influence of K_π is negligible in this case.

Conclusion

Applying the known principles of scaling, linear subsonic and nonlinear transonic similarity rules have been derived for a finite-span jet-flapped wing with partial or full-span

blowing. In deriving the rules, an attempt was made to keep the presentation as general as possible in order to display the interrelation between the linear and nonlinear rules and to allow freedom in adjusting the scaling to emphasize the parameters and type of scaling most appropriate to a particular problem under consideration.

The effect of jet supply pressure ratio was delineated by considering second-order quantities in the jet sheet compatibility condition. The importance of jet supply pressure ratio depends upon the flight Mach number at which the jet nozzle (assuming a convergent configuration) chokes. At this time it is not known whether typical flight vehicles will fall within the parametric spectrum where jet supply pressure ratio is an important consideration. In comparisons with three different sets of wind tunnel data, jet supply pressure ratio was found to be of significant importance for only one set of data considered.

This investigation also disclosed that camber line effects with blowing assume more importance than heretofore was the case in jet-augmented mechanical flap applications.

Finally, although reasonably good agreement was obtained for limited comparisons with experiment for linear subsonic flow, there is a critical need for well-designed wind tunnel experiments to validate both the linear subsonic and nonlinear transonic similarity rules. The experiments should be planned to eliminate tunnel interference effects or should be conducted in a facility where the magnitude of the interference can be accurately predicted. In the tests parametric variations should be made within ranges consistent with the small perturbation assumption of the similarity analysis. Parametric variations also should be specifically tailored to test three-dimensional effects and the nonlinear transonic rules.

Appendix: Second-Order Jet Sheet Compatibility Condition for Compressible Flow

For the jet sheet to be compatible with the external flow, the jet internal static pressures at the sheet upper and lower boundaries must be equal to the corresponding static pressures in the external flow, and the sheet boundaries must be stream surfaces of the external flow. In deriving the compatibility condition, the lateral flow velocity perturbations are assumed to be negligible compared to the vertical and longitudinal ones, thereby permitting the jet sheet flow to be treated as two-dimensional in any plane where $y = a$ constant. A similar assumption is employed by Maskell and Spence[12] in their treatment of a finite-span jet-flapped wing. With reference to Fig. A1, it is also assumed that the jet center line radius of curvature R is large, the jet thickness h is very small, and the downward displacement of the jet is small, such that $h/R \ll 1$ and $R^{-1} \simeq -\partial\theta_{js}/\partial x$.

In jet-flap applications the jet exhaust nozzle height h_j is usually rather small due to the geometrical constraints imposed by the thinness of the airfoil trailing edge. Consequently, for a convergent nozzle, choked (critical) flow may occur if the jet supply pressure is sufficiently high. Assuming the jet sheet internal flow is isentropic, the jet flow downstream of the nozzle will have a differing character for subcritical and supercritical nozzle flow conditions. For subcritical nozzle flows the magnitude of the nozzle exit pressure will be essentially governed by the external freestream static pressure. For the limiting case of zero jet thickness in Spence's incompressible flow analysis,[10] it is implicit that the static pressure along the jet centerline is equal to the freestream static pressure. Woolard[4] has shown that this condition is also approximately true for a first-order compressible flow. If, however, the nozzle flow is supercritical, the nozzle static pressure is governed by the jet supply pressure and may on the average be greater than the freestream static pressure. In the analytical modeling for this case, therefore, some provisions must be made for accounting for the longitudinal decay of the centerline over-pressure

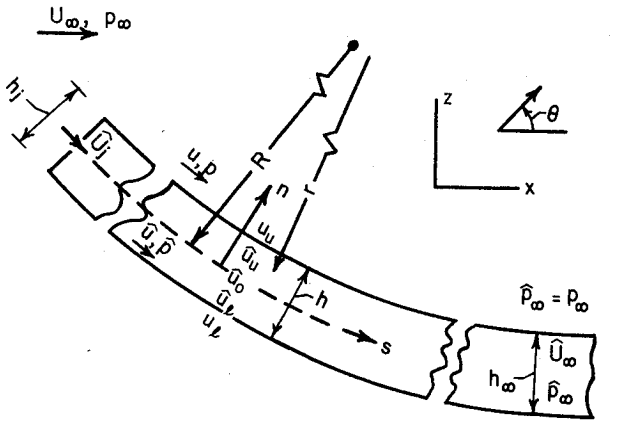

Fig. A1 Notation for the jet sheet.

within the jet. This can be accomplished by a second-order (or higher) analysis of the jet sheet internal flow, as in this Appendix.

With reference to Fig. A1, the internal and external flowfield horizontal velocity components for small perturbations relative to $\hat{U}_\infty$ and U_∞ are given respectively by

$$\hat{u} = \hat{U}_\infty + \hat{u}' \tag{A1}$$

$$u = U_\infty + u' \tag{A2}$$

where $\hat{u}' \ll \hat{U}_\infty$ and $u' \ll U_\infty$.

The irrotationality condition, in natural coordinates (n,s) is[4]

$$(\partial\hat{u}/\partial n)/\hat{u} = 1/r \tag{A3}$$

Expanding r along n gives

$$r \simeq R + (\partial r/\partial n)_0 n + \text{-----} \tag{A4}$$

Substituting Eq. (A4) in Eq. (A3), integrating, and applying the condition $\hat{u} = \hat{u}_0$ at $n = 0$, yields

$$\hat{u}/\hat{u}_0 = \exp[(n/R) - (1/2)(\partial r/\partial n)_0 (n/R)^2 + \text{-----}] \tag{A5}$$

Assuming $[1 - (\partial r/\partial n)_0] \ll 1$ and $(n/R) \ll 1$, making use of Eq. (A1) and expanding Eq. (A5), yields to second order in small quantities

$$\hat{u}' = \hat{u}'_0 + (\hat{U}_\infty + \hat{u}'_0)(n/R) \tag{A6}$$

To an order consistent with nonlinear transonic flow theory, the pressure in the external stream is given by

$$p = p_\infty - \rho_\infty U_\infty^2 (u'/U_\infty) \tag{A7}$$

The jet sheet internal pressure to second order is

$$\hat{p} = \hat{p}_\infty - \hat{\rho}_\infty \hat{U}_\infty^2 [(\hat{u}'/\hat{U}_\infty) + (1/2)(1 - \hat{M}^2)(\hat{u}'/\hat{U}_\infty)^2] \tag{A8}$$

The internal pressures at the upper and lower jet boundaries are given by substituting $\hat{u}_u$ and $\hat{u}_l$ respectively in Eq. (A8), where $\hat{u}'_u$ and $\hat{u}'_l$ are obtained by substituting $n = \pm h/2$ in Eq. (A5). Applying the boundary conditions, $\hat{p}_u = p_u$ and $\hat{p}_l = p_l$, yields to second order

$$p_u - p_l = -\hat{\rho}_\infty \hat{U}_\infty^2 (h/R)[1 + (2 - \hat{M}^2_\infty)(\hat{u}'_0/\hat{U}_\infty] \tag{A9}$$

The variable h/R, which is a function of s, may be determined to second order by applying global continuity between downstream infinity and an arbitrary s-station.[4] Substituting the resulting expression in Eq. (A9), applying center line conditions to Eq. (A8), solving for $(\hat{u}_0'/U_\infty)$, substituting the result in Eq. (A9), and replacing R^{-1} by $-\partial\theta_{js}/\partial x$ yields, to second order[4]

$$p_l - p_u = -C_\pi(\hat{\rho}_\infty \hat{U}_\infty h_\infty)\hat{U}_\infty(\partial\theta_{js}/\partial x) \tag{A10}$$

where

$$C_\pi \equiv 1 - [(\hat{p}_0 - p_\infty)/\gamma\hat{p}_\infty \hat{M}_\infty^2] \tag{A11}$$

Since $\hat{p}_0$ varies with s, the parameter C_π which modifies the usual jet sheet compatibility condition, also varies with s. In order to apply the second-order jet sheet compatibility condition, therefore, $\hat{p}_0(s) \cong \hat{p}_0(x)$ must be determined. Rather than attempt a precise determination some additional approximations will be employed. The rationale for these approximations follow.

Woolard[4] has shown that to first order $\hat{p}_0(s)$ is equivalent to the pressure distribution along the centerline of a thin jet of finite thickness exhausting at zero inclination into a surrounding stream. Consequently, $\hat{p}_0(x)$ can be determined independently of the more general curved jet sheet flow problem. For subcritical nozzle flow into a subsonic external stream, it is well known that $\hat{p}_j = p_\infty$ and hence it is reasonable to take $\hat{p}_0(x) = p_\infty$ for this case. For choked nozzle flow into an incompressible external stream, an approximate solution for $\hat{p}_0(x)$ possibly could be found. With $\hat{p}_0(x)$ then known, Spence's integral equations[10] could be appropriately modified and possibly solved. The resulting solutions could be extended to subsonic linear compressible flow by means of the similarity relations herein. The solutions so obtained would be functions of the supply duct pressure ratio $(\hat{P}/p_\infty)$ in addition to c_j. Note, however, that the present analysis is a small perturbation one, for which $(\hat{p}_0 - p_\infty)/\gamma p_\infty M_\infty^2 \ll 1.0$, from which it follows that $C_\pi \to 1.0$. With this in mind, it hardly seems worthwhile to treat C_π as a variable. Instead, an average $\langle C_\pi \rangle$ will be sought such that $\langle C_\pi \rangle$ has a unity value for subcritical nozzle pressure ratios and a constant non-unity value for critical and supercritical nozzle pressure ratios. To determine $\langle C_\pi \rangle$ for the choked nozzle flow case, assume that

$$\langle \hat{p}_0 \rangle = \tfrac{1}{2}(\hat{p}_j + \hat{p}_\infty) \equiv \tfrac{1}{2}(\hat{p}_* + p_\infty) \tag{A12}$$

Substituting $\langle \hat{p}_0 \rangle$ for p_0 in Eq. (A11) yields

$$\langle C_\pi \rangle \equiv 1 - [(\hat{p}_*/p_\infty) - 1]/2\gamma\hat{M}_\infty^2 \tag{A13}$$

For subcritical nozzle flow, the flowfield across the nozzle is affected by the external stream, generally is nonuniform, and therefore is inappropriate for use as a reference stream about which to perform a perturbation analysis. In the preceding analysis this is one reason for selecting the jet internal flow at downstream infinity as the reference stream for the perturbation analysis (see Eq. (A1)). For choked or supersonic nozzle flow, the details of the flow across the nozzle are governed by the upstream conditions in the nozzle duct, and the duct contours can be designed to give a uniform flow at the nozzle exit. Hence, from the standpoint of flow uniformity the nozzle exit flow can be used as a reference stream. However, for this case, when the nozzle flow is sonic, the assumption of small perturbations is locally invalid. This, then, is a second reason for employing the downstream jet flow as a reference stream in the previous perturbation analyses. Tentatively, disregarding the second reason, a perturbation analysis relative to a choked nozzle stream can be employed to yield additional insight regarding $<C_\pi>$. Such an analysis yields[4] to second order, the result

$$p_l - p_u = -C_\pi'(\hat{\rho}_\infty \hat{U}_\infty h_\infty)\hat{U}_\infty(\partial\theta_{js}/\partial x) \tag{A14}$$

where

$$C_\pi' \equiv 1 - [(\hat{p}_0 - p_\infty)/2\gamma\hat{p}_*] \tag{A15}$$

If, as before, a mean value of p_0 given by Eq. (A12) is employed in Eq. (A15), the mean value of C_π' is

$$\langle C_\pi' \rangle \equiv 1 - [(\hat{p}_* - p_\infty)/2\gamma\hat{p}_*] \tag{A16}$$

It is found that, $\langle C_\pi \rangle \simeq \langle C_\pi' \rangle$ for $(\hat{P}/\hat{p}_*) \leq (\hat{P}/p_\infty) \leq 5$, where $\langle C_\pi \rangle$ and $\langle C_\pi' \rangle$ differ from each other by less than 3%. In view of its simpler form, $\langle C_\pi' \rangle$ will be employed. The second-order jet sheet compatibility condition then becomes

$$C_{p_l} - C_{p_u} = -K_\pi c_j c(\partial\theta_{js}/\partial x) \tag{A17}$$

where

$$K_\pi = 1.0 \text{ for } (\hat{P}/p_\infty) \leq (\hat{P}/\hat{p}_*) \tag{A18}$$

$$K_\pi = 1 - (2\gamma)^{-1}\{1 - [(\hat{P}/\hat{p}_*)/(\hat{P}/p_\infty)]\}$$

for

$$(\hat{P}/\hat{p}_*) \leq (\hat{P}/p_\infty) \leq 5 \tag{A19}$$

and the symbol $\langle C_\pi' \rangle$ has been replaced by K_π. The critical pressure ratio is given by

$$(\hat{P}/\hat{p}_*) = (1/2 + \gamma/2)^{\gamma/\gamma-1} \tag{A20}$$

The second-order effect is reflected in the parameter K_π such that the second-order jet momentum coefficient is effectively $(K_\pi c_j)$. Below the critical pressure ratio $K_\pi = 1$ and there is no second-order effect.

References

[1] Siestrunk, R., "General Theory of the Jet Flap in Two-Dimensional Flow," *Boundary Layer and Flow Control*, Vol. 1, G. V. Lachman, ed., Pergamon Press, New York, 1961, p. 359.

[2] Levinsky, E.S., "Prandtl-Glauert Rule for Wings with Jet Flaps," General Dynamics/Convair Aerospace Div., Aero TN-73-AE-11, June 1973.

[3] Elzweig, S., "Subsonic Similarity Rule for Jet-Flapped Airfoil," *Journal of Aircraft*, Vol. 8, Sept. 1971, pp. 744-745.

[4] Woolard, H.W., "Subsonic and Transonic Similarity Rules for Jet-Flapped Wings," AFSC, AFFDL, WPAFB, OH, Report AFFDL-TR-76-86 (AD A033 550), Aug. 1976.

[5] Spreiter, J.R., "On the Application of Transonic Similarity Rules to Wings of Finite Span," NACA Report 1153, 1953.

[6] Grahame, W.E. and Headley, J.W., "Jet Flap Investigation at Transonic Speeds," AFSC, AFFDL, WPAFB, OH, Report AFFDL-TR-69-117 (AD 865 697), Feb. 1970.

[7] Peake, D.J., Yoshihara, H., Zonars, D., and Carter, W., "The Transonic Performance of Two-Dimensional, Jet-Flapped Aerofoils at High Reynolds Numbers," in AGARD Conference Proceedings No. 83, *Facilities and Techniques for Aerodynamic Testing at Transonic Speeds and High Reynolds Number*, AGARD CP-83-71 (N72-11854), Aug. 1971.

[8] Malavard, L., Poisson-Quinton, Ph, and Jousserandot, P., "Jet-Induced Circulation Control, Part II—Experimental Results," *Aero Digest*, Vol. 72, No. 4, Oct. 1956, pp. 46-59.

[9] Woolard, H.W. and Niehaus, Bernard F., "Cambered Jet-Flapped Airfoil Theory with Tables and Computer Programs for Application," AFSC, AFFDL, WPAFB, OH, Report AFFDL-TR-77-63 (AD A048 528), Sept. 1977.

[10] Spence, D.A., "The Lift Coefficient of a Thin Jet-Flapped Wing," *Proceedings of Royal Society of London*, Ser. A, Vol. 238, No. 1212, Dec. 1956.

[11] Hartunian, R.A., "The Finite Aspect Ratio Jet Flap," Cornell Aeronautical Laboratory, Report A1-1190-A-3, Oct. 1959.

[12] Maskell, L.C. and Spence, D.A., "A Theory of the Jet Flap in Three Dimensions," *Proceedings of the Royal Society of London*, Ser. A Vol. 251, 1959.